Supporting Information

Descriptors for Electrochemical CO_2 Reduction in Imidazolium-Based Electrolytes

Federico Dattila[1], Alessia Fortunati[1†], Federica Zammillo[1], Hilmar Guzmán[1], Núria López[2], Simelys Hernández[1*]*

[1] CREST Group, Department of Applied Science and Technology (DISAT), Politecnico di Torino, Corso Duca degli Abruzzi 24, 10129, Turin, Italy

[2] Institute of Chemical Research of Catalonia (ICIQ), The Barcelona Institute of Science and Technology (BIST), Avinguda dels Països Catalans 16, 43007, Tarragona, Spain

[†] Present Address: Istituto Italiano di Tecnologia, Via Livorno 60, 10144 Torino, Italy

Corresponding authors: nlopez@iciq.es; simelys.hernandez@polito.it

CONTENTS

1. EXPERIMENTAL METHODS S2
2. COMPUTATIONAL DETAILS S6
3. SUPPORTING TABLES S7
4. SUPPORTING FIGURES S9
5. REFERENCES S18

1. EXPERIMENTAL METHODS

Chemicals. The electrochemical studies were performed using imidazolium-based ionic liquids by IOLITEC GmbH (high purity grade, above 99% for triflates, above 98% for alkenoates). The water content was kept below 100 ppm for the triflates, below 0.5% for the alkanoates, and in the range of 0.6–0.8% for the acetate anion. Acetonitrile (ACN) was purchased from Sigma Aldrich (≥99.9%, gradient grade, suitable for HPLC), with water content ≤ 0.02%. Further details are provided in the original experimental work.[1]

Electrochemical cell and set-up. The electrochemical CO_2R tests were carried out in a two-compartment (H-type) cell. Commercial silver foil (99.999% purity) was employed as working electrodes (WE) with a total geometric area of 3 cm^2 (1.5 cm^2 on each side), while Ag/AgCl in saturated KCl was chosen as the reference electrode (RE). Both working and reference electrodes were immersed in 40 mL of 0.3 M IL in acetonitrile (ACN) to decrease pure IL viscosity and improve CO_2 solubility. The anodic reaction (Oxygen Evolution Reaction, OER) was carried out through a nickel mesh (counter electrode, CE) immersed in an aqueous solution of potassium hydroxide (40 mL of 0.1 M KOH). The cell chambers were separated by a commercial bipolar membrane (BM, Fumasep^{TM} FBM by Fumatech), consisting of an anion exchange layer (AEL) and a cation exchange layer (CEL) which faced the anode and cathode compartments of the cell, respectively. The membrane was stored in a saturated solution of sodium chloride. It was activated before each use through rinsing in a solution of H_2SO_4 0.1 M (cation exchange side) and KOH 0.1 M (anion exchange side) already assembled in the H-cell.

Electrocatalytic CO_2R tests in acetonitrile. During the electrochemical measurements, the N_2 and CO_2 were bubbled directly in the electrolyte solution of the cathodic compartment at a constant rate (20 NmL/min, *i.e.* at normal temperature, 293.15 K, and pressure, 1 atm), defined by a mass

flow controller (Bronkhorst EL-FLOW). To facilitate CO_2 dissolution and diffusion, the electrolyte was magnetically stirred. Before the electrochemical tests, the solution was outgassed with N_2 and then saturated with CO_2. Chronopotentiometry (CP) measurements were carried out through a VoltaLab PGZ 301 Dynamic Potentiostat equipped with VoltaMaster 4 at different applied current densities for a duration of 2 hours. Before each CP, the Ag foil was cleaned through the following protocol: sonication in ultrasound bath in acetonitrile, rinse with water, and drying under nitrogen flow. The in-line analysis of the gaseous products evolved during CP was carried out with a Varian 490 Micro GC equipped with a PPQ and a Molesieve columns.

Electrochemical surface area (ECSA) measurements in acetonitrile. Cyclic voltammetry (CV) measurements were carried out to determine the double layer capacitance (C_{DL}) of the electrode/electrolyte interface in each solution in a potential range where no Faradaic process occurs, both in N_2 and CO_2 saturated electrolytes. In particular, the CVs were performed over a potential window of $\pm$ 0.1 V around the open circuit voltage (OCV) with scan rates of 5, 10, 25, 50, 75 and 100 mV s^{-1}. These measurements were carried out at ambient conditions in a three-electrode single cell, comprised of an Ag foil, Ni foil and Ag/AgCl in saturated KCl as working, counter, and reference electrode respectively. The gas flow (N_2 and CO_2) was kept constant *via* a mass flow controller at 20 NmL min^{-1}. At each scan rate, the current densities were recorded in both the anodic and cathodic regions of the CV at the point corresponding to the OCV of the working electrode. The absolute mean of these current densities can be credited to the charging current, j_{charging}, of the electrochemical double layer, which is linearly related to the scan rate, ν, with the slope equal to the C_{DL} (Supporting Equation 1). Once all double layer capacitances were established, the C_{DL} of the Ag foil in pure ACN solutions were defined as the reference capacitances, $C_{\mathrm{DL,ref}}$ (12.11 μF cm^{-2} and 12.91 μF cm^{-2} under N_2 and CO_2 environments,

respectively). Then, the relative roughness factor was determined for each electrolyte, under each respective gas environment through Supporting Equation 2. Finally, the ECSA was obtained from Supporting Equation 3, where A_{geom} represents the geometric area of the electrode exposed to the electrolyte.

$$C_{\text{DL}} = \frac{j_{\text{charging}}}{v} \qquad \text{Supporting Equation 1}$$

$$R_{\text{f}} = \frac{C_{\text{DL}}}{C_{\text{DL,ref}}} \qquad \text{Supporting Equation 2}$$

$$\text{ECSA} = A_{\text{geom}}\, R_{\text{f}} \qquad \text{Supporting Equation 3}$$

Electrocatalytic CO_2R tests on mixtures of ionic liquids in 3-methoxypropionitrile. Pure [BMIM][SO_3CF_3] and [BMIM][CO_2CH_3] notably exhibit high viscosity. As such, when considering their application in electrochemical processes, diluting these ILs with a suitable solvent is imperative. In the experimental study discussed in this section, the solvent of choice was 3-methoxypropionitrile (3MPN). We carried out a systematic protocol to determine the optimal concentration of the ionic liquid within 3MPN. Pure solvent was added to pure ionic liquids and subsequently the conductivity of the resulting solutions was measured. The maximum conductivity was attained by [BMIM][SO_3CF_3] and [BMIM][CO_2CH_3] when dissolved in 3MPN. Specifically, [BMIM][SO_3CF_3] achieved its highest conductivity, σ = 16 mS cm^{-1}, at a concentration of [IL] = 1.6 M, while [BMIM][CO_2CH_3] reached its peak conductivity value of σ = 5.6 mS cm^{-1} at a molar concentration of [IL] = 2.4 M.

The solutions containing [BMIM][SO_3CF_3] and [BMIM][CO_2CH_3] at their maximum conductivity were combined in the absence and presence of water to investigate their CO_2 absorption capacity and determine the most effective CO / H_2 ratio. Various combinations of ILs

were prepared as outlined in Supporting Table 4. The experimental electrochemical setup used to test the selectivity in the electrocatalytic reduction process of CO_2 was analogous to the catholyte compartment of the H-type cell mentioned in *Experimental methods* section.

2. COMPUTATIONAL DETAILS

The density functional theory calculations were done by means of the Vienna Ab Initio Simulation Package (VASP)[2,3] through the PBE density functional.[4] To account for van der Waals interactions, dispersion was included through the DFT-D2 method,[5,6] with the parametrization of C_6 coefficients for metals.[7] Inner electrons were represented by PAW pseudopotentials[8,9] and the monoelectronic states for the valence electrons expanded as plane waves with a kinetic energy cutoff of 450 eV.

The experimental catalyst (polycrystalline silver foil) was modelled as Ag(111) p(3×3) supercell (Figure 3a). Such cell included at least four layers, with the two uppermost fully relaxed to resemble the surface and the rest fixed to the bulk distances. Seven ionic liquids complexes were assessed, with $EMIM^+$ ($BMIM^+$) as cations and acetate, trifluoroacetate, triflate, tetrafluoroborate, and pentafluorophenol as anions (see Figure 3b). The Brillouin zone was sampled by a Γ-centered k-points mesh from the Monkhorst-Pack method,[10] with a reciprocal grid size smaller than 0.03 $Å^{-1}$. The vacuum between the slabs was larger than 16 Å to prevent spurious periodic interactions between ionic liquid and bulk of the next cell. The $EMIM^+$ ($BMIM^+$)-anion complex was placed only on one side of the slab, in line with other DFT studies on ILs,[1,11–13] thus a dipole correction was included in the simulation to account for artificial contributions from the asymmetric slab model.[14] All energies are reported using as references the Ag(111) p(3×3) surface plus the relative $EMIM^+$ ($BMIM^+$)-anion complex far away from the surface (> 5 Å, see Figure 3a). When required, the relative energy between the H^+ and the H_2(g) at $U = 0$ V was obtained with the Computational Hydrogen Electrode.[15,16]

3. SUPPORTING TABLES

Supporting Table 1: Composition of BMIM-based solutions in ACN. Total $V_{Catholyte}$ = 40 mL. [IL]=0.3 M in ACN.

Ionic liquid (IL)	**IL**	**ACN (mL)**	**H_2O (mL)**
[BMIM][SO_3CF_3]	2.7 mL	37.3	0
[BMIM][BF_4]	2.1 mL	37.9	0
[BMIM][CO_2CF_3]	2.5 mL	37.5	0
[BMIM][CO_2CH_3]	2.3 mL	37.7	0
[BMIM][5FF]	3.9 g	Up to the 40 mL mark	0

Supporting Table 2: Composition of EMIM-based solutions in acetonitrile. Total $V_{Catholyte}$ = 40 mL, [IL] = 0.3M in ACN.

Ionic liquid (IL)	**IL (mL)**	**ACN (mL)**	**H_2O (mL)**
[EMIM][SO_3CF_3]	2.3	37.3	0
[EMIM][CO_2CH_3]	1.8	37.2	0

Supporting Table 3: Summary of double layer capacitances and roughness factors for tested electrolytes.

Electrolyte	Geometric Area (cm^2)	C_{DL} ($\mu F\ cm^{-2}$)		Roughness Factor		ECSA (cm^2)	
		N_2	CO_2	N_2	CO_2	N_2	CO_2
0.3 M [BMIM][SO_3CF_3] in ACN	1.08	78.48	86.22	6.48	6.68	7.00	7.21
0.3 M [BMIM][CO_2CH_3] in ACN	0.84	26.00	34.92	2.15	2.71	1.81	2.28
0.3 M [EMIM][SO_3CF_3] in ACN	1.08	93.35	89.92	7.71	7.52	8.33	8.12
0.3 M [EMIM][CO_2CH_3] in ACN	1.08	57.04	41.20	4.71	3.19	5.09	3.45

Supporting Table 4: Blend solutions that incorporate varying volume proportions of [BMIM][SO_3CF_3], [BMIM][CO_2CH_3], and H_2O in 3-MPN as the solvent.

ILs Mix	[BMIM][SO_3CF_3] (mL)	[BMIM][CO_2CH_3] (mL)	H_2O (mL)	σ_{TOT} ($mS\ cm^{-1}$)
1	40.0	10.0	0	14.9
2	30.0	10.0	10	21.0
3	20.o	10.0	20	18.5
4	23.3	11.6	15	24.0

4. SUPPORTING FIGURES

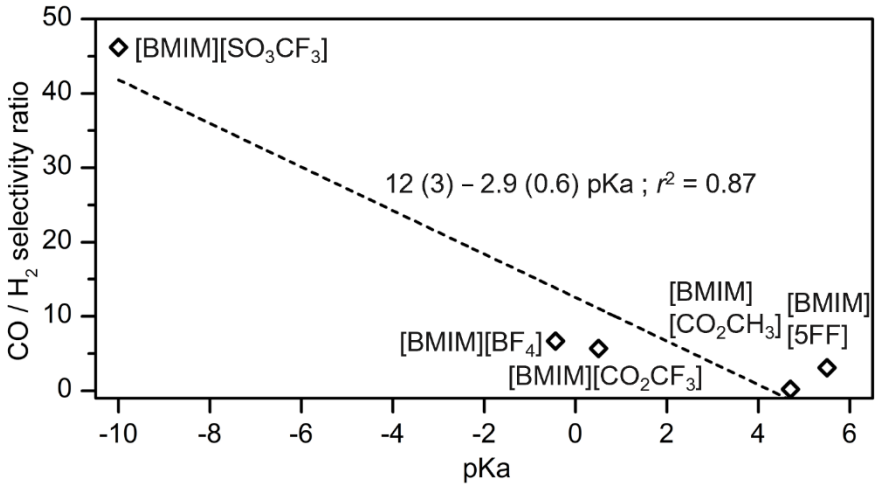

Supporting Figure 1. Linear correlation between CO / H_2 ratio at j_{tot} = –20 mA cm^{-2} and the pKa of anions (calculated in aqueous media). Fit parameters are given as inset.

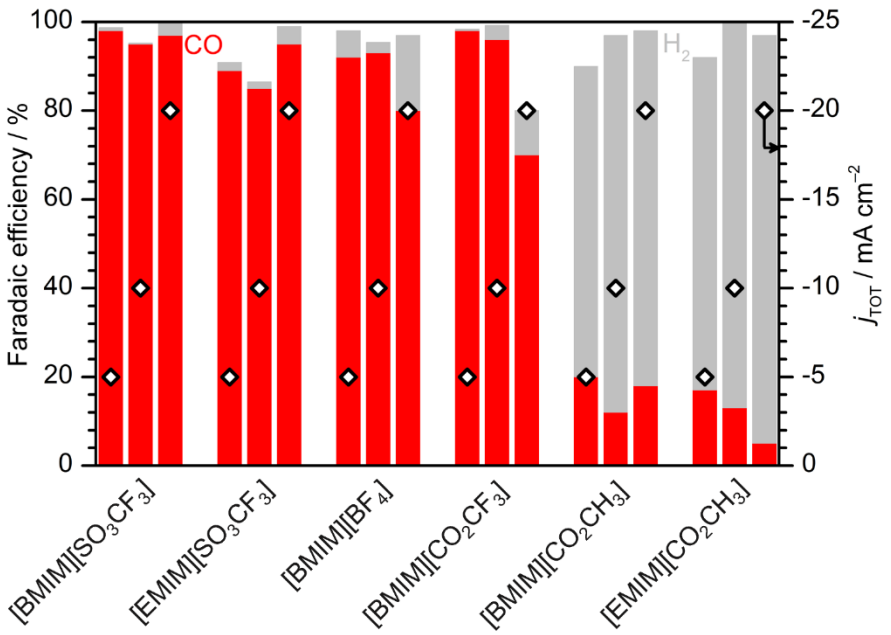

Supporting Figure 2. Experimental results for CO_2 reduction on silver foil in imidazolium-based ionic liquids. Faradaic efficiency toward CO is reported in red, while H_2 selectivity is indicated in gray. Three values of current densities were applied (–5, –10, –20 mA cm^{-2}), as indicated by rhomboidal data points (left y-axis). The experimental set-up consisted of H-cell, Ag foil as working electrode, Ni mesh as counter electrode, 0.3 M IL in ACN as catholyte, 0.1 M KOH as anolyte. Data taken from ref 1.

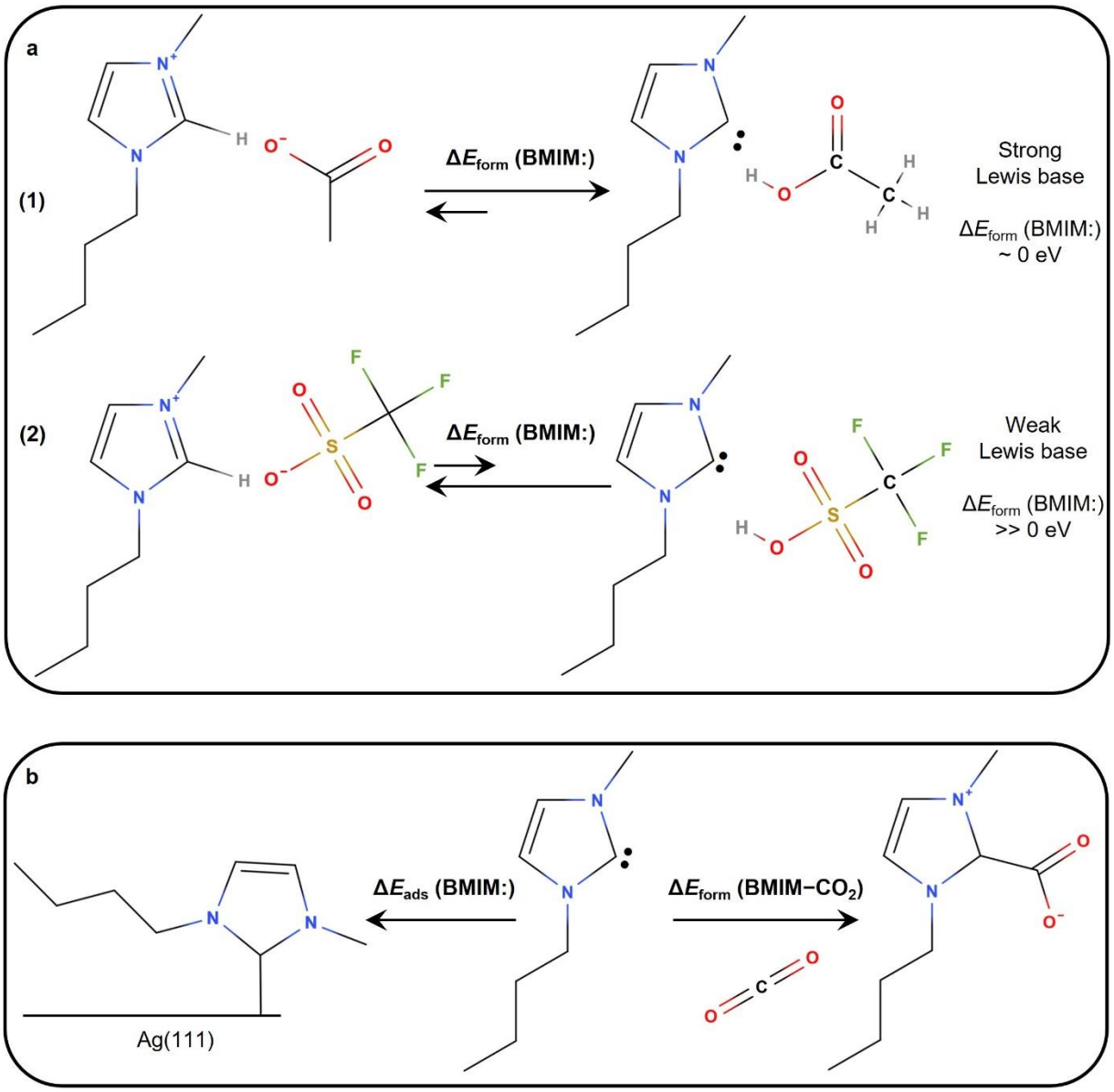

Supporting Figure 3. (a) Formation of carbenes from the homogeneous reaction between $BMIM^+$ and anion species. The formation energy of carbene, ΔE_{form} (BMIM:), depends on anion basicity. (b) Reactions of carbenes with Ag(111) and CO_2. Once formed, carbenes can either adsorb on the catalytic surface, thus poisoning it, or capture CO_2 from the solution, thus forming a carboxylate complex.

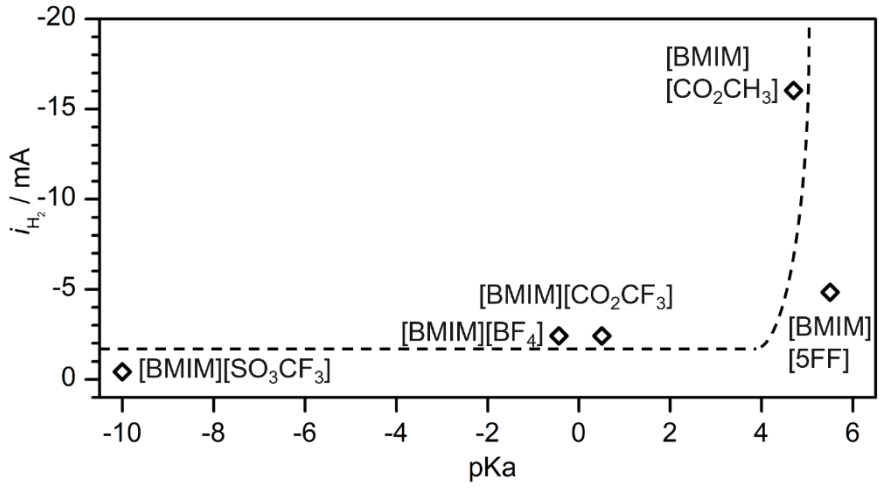

Supporting Figure 4. Dependence of the partial current toward hydrogen on the pKa of anions (in aqueous media). The dashed line serves as a guide for the eye and reproduces a Langmuir isotherm. The total applied current density was –20 mA cm^{-2}.

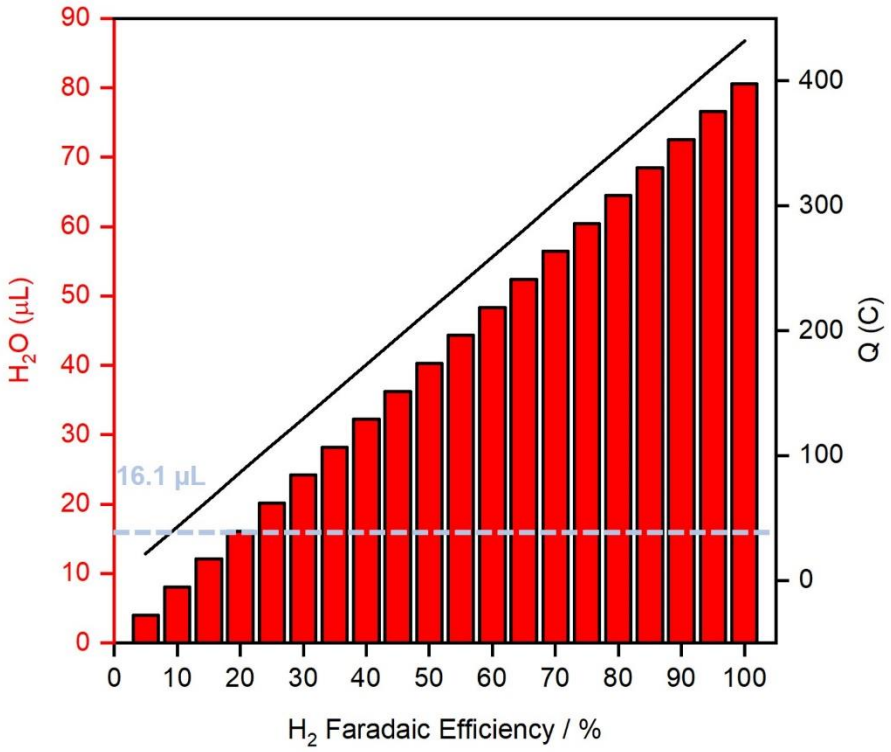

Supporting Figure 5. Estimated H_2O consumption for 2h CO_2R depending on H_2 Faradaic Efficiency for an applied current density of –20 mA/cm^2. The dashed line indicates the difference in Faradaic Efficiency due to H_2O impurities in acetate-based ionic liquids. At the right y-axis, the overall charge required to reduce H_2O to H_2 along the 2h. Electrode geometric area is assumed to be 3 cm^2, while the Faradaic constant is 96485 C/mol.

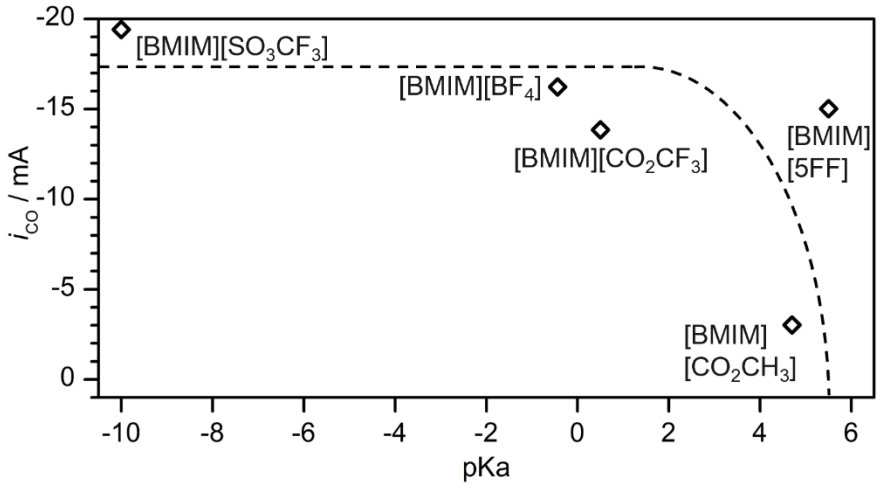

Supporting Figure 6. Dependence of the partial current toward carbon monoxide on the pKa of anions (in aqueous media). The dashed line serves as a guide for the eye and reproduces a Langmuir isotherm. The total applied current density was –20 mA cm^{-2}.

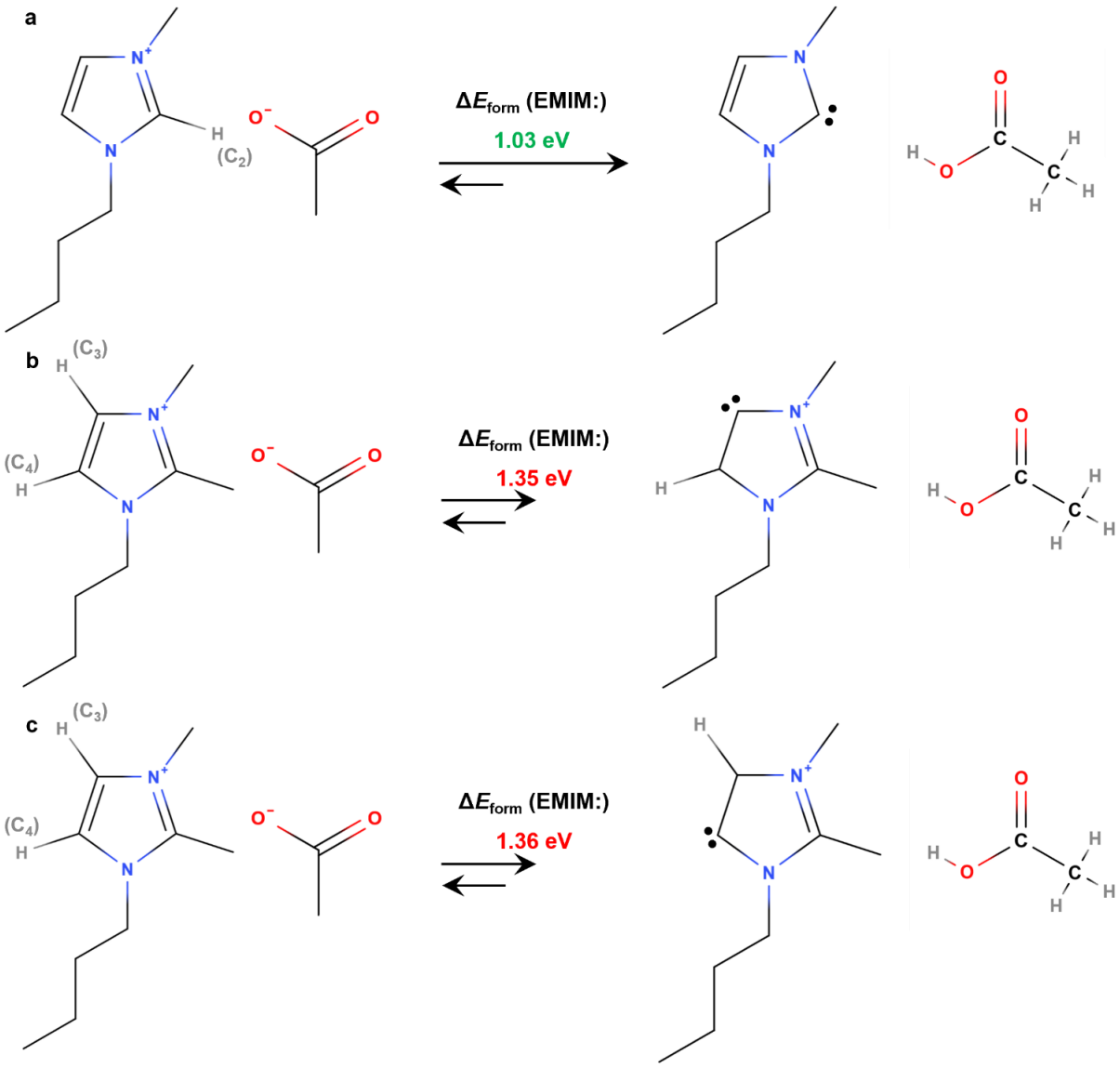

Supporting Figure 7. Formation of carbenes from the homogeneous reaction of (a) $BMIM^+$ (C_2-H release) and (b), (c) methylated-$BMIM^+$ with acetate (C_3-H and C_4-H releases). The formation energy of carbene, ΔE_{form} (BMIM:), is reported in eV.

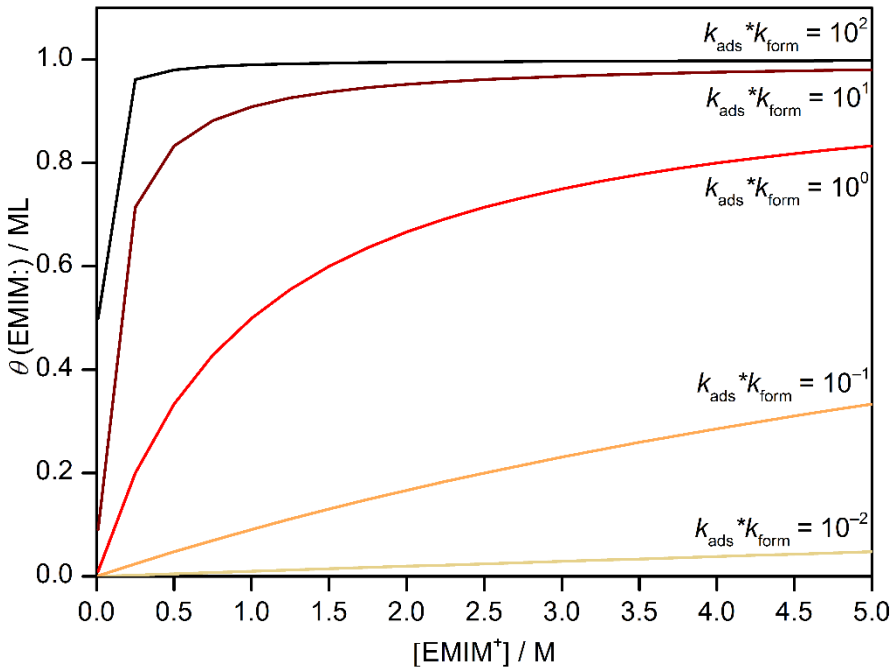

Supporting Figure 8. Dependence of surface coverage of carbenes (EMIM:) on the bulk concentration of cations ($EMIM^+$) at different rates of formation (k_{ads}) and adsorption (k_{form}) of carbenes.

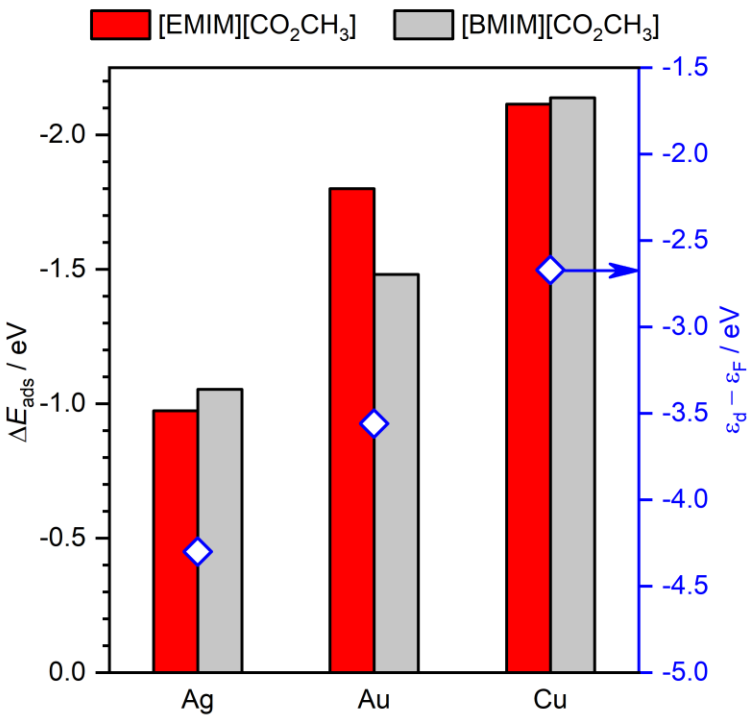

Supporting Figure 9. Adsorption energies of carbenes (EMIM: in red, BMIM: in grey) on Ag(111) p(3×3), Au(111) p(3×3), and Cu(111) p(3×3) respectively in the presence of [CO_2CH_3] as IL anion. Blue data points represent the metal *d*-band centre (right *y*-axis).

5. REFERENCES

(1) Fortunati, A.; Risplendi, F.; Re Fiorentin, M.; Cicero, G.; Parisi, E.; Castellino, M.; Simone, E.; Iliev, B.; Schubert, T. J. S.; Russo, N.; Hernández, S. Understanding the Role of Imidazolium-Based Ionic Liquids in the Electrochemical CO_2 Reduction Reaction. *Commun. Chem.* **2023**, *6*, 84. https://doi.org/10.1038/s42004-023-00875-9.

(2) Kresse, G.; Furthmüller, J. Efficiency of Ab-Initio Total Energy Calculations for Metals and Semiconductors Using a Plane-Wave Basis Set. *Comput. Mater. Sci.* **1996**, *6*, 15–50. https://doi.org/10.1016/0927-0256(96)00008-0.

(3) Kresse, G.; Furthmüller, J. Efficient Iterative Schemes for Ab Initio Total-Energy Calculations Using a Plane-Wave Basis Set. *Phys. Rev. B* **1996**, *54*, 11169–11186. https://doi.org/10.1103/PhysRevB.54.11169.

(4) Perdew, J. P.; Burke, K.; Ernzerhof, M. Generalized Gradient Approximation Made Simple. *Phys. Rev. Lett.* **1996**, *77*, 3865–3868. https://doi.org/10.1103/PhysRevLett.77.3865.

(5) Grimme, S. Semiempirical GGA-Type Density Functional Constructed with a Long-Range Dispersion Correction. *J. Comput. Chem.* **2006**, *27*, 1787–1799. https://doi.org/10.1002/jcc.20495.

(6) Bucko, T.; Hafner, J.; Lebègue, S.; Ángyán, J. G.; Bučko, T.; Hafner, J.; Lebegue, S.; Angyán, J. G. Improved Description of the Structure of Molecular and Layered Crystals: Ab Initio DFT Calculations with van Der Waals Corrections. *J. Phys. Chem. A* **2010**, *114*, 11814–11824. https://doi.org/10.1021/jp106469x.

(7) Almora-Barrios, N.; Carchini, G.; Błoński, P.; López, N. Costless Derivation of Dispersion Coefficients for Metal Surfaces. *J. Chem. Theory Comput.* **2014**, *10*, 5002–5009. https://doi.org/10.1021/ct5006467.

(8) Blöchl, P. E. Projector Augmented-Wave Method. *Phys. Rev. B* **1994**, *50*, 17953–17979. https://doi.org/10.1103/PhysRevB.50.17953.

(9) Kresse, G.; Joubert, D. From Ultrasoft Pseudopotentials to the Projector Augmented-Wave Method. *Phys. Rev. B* **1999**, *59*, 1758–1775. https://doi.org/10.1103/PhysRevB.59.1758.

(10) Monkhorst, H. J.; Pack, J. D. Special Points for Brillouin-Zone Integrations. *Phys. Rev. B* **1976**, *13*, 5188–5192. https://doi.org/10.1103/PhysRevB.16.1748.

(11) Urushihara, M.; Chan, K.; Shi, C.; Nørskov, J. K. Theoretical Study of $EMIM^+$ Adsorption on Silver Electrode Surfaces. *J. Phys. Chem. C* **2015**, *119*, 20023–20029. https://doi.org/10.1021/acs.jpcc.5b07268.

(12) Chen, L. D.; Urushihara, M.; Chan, K.; Nørskov, J. K. Electric Field Effects in Electrochemical CO_2 Reduction. *ACS Catal.* **2016**, *6*, 7133–7139. https://doi.org/10.1021/acscatal.6b02299.

(13) Ortuño, M. A.; Hollóczki, O.; Kirchner, B.; López, N. Selective Electrochemical Nitrogen Reduction Driven by Hydrogen Bond Interactions at Metal-Ionic Liquid Interfaces. *J. Phys. Chem. Lett.* **2019**, *10*, 513–517. https://doi.org/10.1021/acs.jpclett.8b03409.

(14) Makov, G.; Payne, M. C. Periodic Boundary Conditions in Ab Initio Calculations. *Phys. Rev. B* **1995**, *51*, 4014–4022. https://doi.org/10.1103/PhysRevB.51.4014.

(15) Peterson, A. A.; Abild-Pedersen, F.; Studt, F.; Rossmeisl, J.; Nørskov, J. K. How Copper Catalyzes the Electroreduction of Carbon Dioxide into Hydrocarbon Fuels. *Energy Environ. Sci.* **2010**, *3*, 1311–1315. https://doi.org/10.1039/c0ee00071j.

(16) Nørskov, J. K.; Rossmeisl, J.; Logadottir, A.; Lindqvist, L.; Kitchin, J. R.; Bligaard, T.; Jónsson, H. Origin of the Overpotential for Oxygen Reduction at a Fuel-Cell Cathode. *J. Phys. Chem. B* **2004**, *108*, 17886–17892. https://doi.org/10.1021/jp047349j.